Agyeman MO, Vien QT, Ahmadinia A, Yakovlev A, Tong KF, Mak T. A Resilient 2-D Waveguide Communication Fabric for Hybrid Wired-Wireless NoC Design. *IEEE Transactions on Parallel and Distributed Systems* 2017, 28(2), 359-373.

Copyright:

DOI link to article:

Date deposited:

13/02/2017

A Resilient 2-D Waveguide Communication Fabric for Hybrid Wired-Wireless NoC Design

Michael Opoku Agyeman, *Member, IEEE*, Quoc-Tuan Vien, *Member, IEEE*,
Ali Ahmadinia, *Member, IEEE*, Alexandre Yakovlev, *Senior Member, IEEE*,
Kin-Fai Tong, *Member, IEEE*, and Terrence Mak, *Member, IEEE*

Abstract—Hybrid wired-wireless Network-on-Chip (WiNoC) has emerged as an alternative solution to the poor scalability and performance issues of conventional wireline NoC design for future System-on-Chip (SoC). Existing feasible wireless solution for WiNoCs in the form of millimeter wave (mm-Wave) relies on free space signal radiation which has high power dissipation with high degradation rate in the signal strength per transmission distance. Moreover, over the lossy wireless medium, combining wireless and wireline channels drastically reduces the total reliability of the communication fabric. Surface wave has been proposed as an alternative wireless technology for low power on-chip communication. With the right design considerations, the reliability and performance benefits of the surface wave channel could be extended. In this paper, we propose a surface wave communication fabric for emerging WiNoCs that is able to match the reliability of traditional wireline NoCs. First, we propose a realistic channel model which demonstrates that existing mm-Wave WiNoCs suffers from not only free-space spreading loss (FSSL) but also molecular absorption attenuation (MAA), especially at high frequency band, which reduces the reliability of the system. Consequently, we employ a carefully designed transducer and commercially available thin metal conductor coated with a low cost dielectric material to generate surface wave signals with improved transmission gain. Our experimental results demonstrate that the proposed communication fabric can achieve a 5 dB operational bandwidth of about 60 GHz around the center frequency (60 GHz). By improving the transmission reliability of wireless layer, the proposed communication fabric can improve maximum sustainable load of NoCs by an average of 20.9 and 133.3 percent compared to existing WiNoCs and wireline NoCs, respectively.

Index Terms—Hybrid wired-wireless Network-on-Chip, reliability, surface wave, mm-Wave, WiNoC, waveguide, wireless channel

✦

1 INTRODUCTION

To compensate for the fast-paced technological scalability with the performance bottleneck of conventional metal based interconnects (wireline), the research for alternative interconnect fabrics such as optical networks, three dimensional integrated circuits (3-D ICs) and millimeter wave (mm-wave) has emanated for emerging System-on-Chip (SoC) design [1], [2]. In optical interconnects a photon needs to be converted back to electrons to be stored in the electronic circuitry. Consequently, optical networks have a high design complexity as well as high power, area, and latency

overheads. On the other hand, though 3-D ICs are Complementary Metal Oxide Semiconductor (CMOS) compatible and have shorter vertical links with enhanced scalability, 3D integration is still in its infancy due to alignment, low yield and high temperature dissipation issues in the current technology which lowers the reliability of system [3].

RF interconnect has low area and low power consumption due to its CMOS compatibility. However, RF interconnect relies on long transmission lines for guided data transmission which requires alignment between transmission pairs. mm-Wave, has emerged as a more feasible solution with promising CMOS components that can scale with transistor technology. However, the on-chip antennas and transceivers have non-negligible area and power overheads. Conventional wireline based NoCs on the other hand, are highly efficient for short distances despite their limitations over long distance. Consequently, hybrid wired-wireless Networks-on-Chip (WiNoCs) have emerged to combine the global performance benefits of mm-Wave as well as the short range low power and area benefits of the wireline communication fabric in NoCs. However the wireless communication fabric is lossy and hence lowers the overall reliability of WiNoCs [4], [5], [6]. Conventional wires have extremely low bit error rate (BER) of around 10^{-14} compared to that of mm-Wave (around 10^{-7}). Moreover, the E-field decay rate of the mm-Wave can be expressed as

$$E_{decay} \propto \frac{1}{d}, \tag{1}$$

- M. Opoku Agyeman is with the Computing and Immersive Technologies, University of Northampton, Northampton NN2 6JB, United Kingdom. E-mail: Michael.OpokuAgyeman@northampton.ac.uk.
- Q.-T. Vien is with the School of Science and Technology, Middlesex University, London NW4 4BT, United Kingdom. E-mail: q.vien@mdx.ac.uk.
- A. Ahmadnia is with the Department of Computer Science, California State University San Marcos, San Marcos, CA 92096. E-mail: aahmadinia@csusm.edu.
- A. Yakovlev is with the School of EECE, University of Newcastle upon Tyne, Newcastle upon Tyne, Tyne and Wear NE1 7RU, United Kingdom. E-mail: alex.yakovlev@newcastle.ac.uk.
- K.-F. Tong is with the Department of Electrical and Electronic Engineering, UCL, London NE1 7RU, United Kingdom. E-mail: K.tong@ucl.ac.uk.
- T. Mak is with the School of Electronics and Computer Science, University of Southampton, Southampton NE1 7RU, United Kingdom. E-mail: tmak@ecs.soton.ac.uk.

where d is the separation between the transmitting and the receiving nodes. Consequently, the transmit signal loss on the wireless layer is significantly high. Also, the radiation patterns of the antenna for existing wireless NoCs is limited by a distance of up to 23 mm with significantly high power dissipation and losses due to free space propagation [7]. In NoCs, a single message loss can have drastic effects on the performance of the multi-core system. To improve the reliability of existing WiNoCs, error-control-coding (ECC) [1], network coding (NC) [8], retransmission schemes [4], adaptive routing [9], [10] in 3D NoCs with capacitive and inductive coupling links [11] could be employed. However, these techniques rely on the underlying lossy wireless communication fabric for retransmission of handshake signals, erroneous and non-erroneous packets. Therefore, the throughput of WiNoCs is reduced due to the extra timing overhead and retransmitted packets in the network. Hence, novel wireless communication fabrics that offer high data bandwidth as well as improved reliability with BER similar to the wired communication fabric are required to provide a good trade-off for WiNoCs.

Wireless communication fabric based on the Zenneck surface wave (SW) concept has been proposed as an emerging wireless communication fabric that is power efficient with improved data throughput for long distance communication [12]. The surface wave propagates on a specially designed sheet which is an inhomogeneous plane that supports electromagnetic wave transmission. The signal generated in the 2-D sheet can traverse in all directions providing a natural fan-out feature for supporting realistic on-chip applications such as cache coherency where multicast is dominant. Moreover, a transceiver used in traditional RF or millimeter wave design can be employed for surface wave propagation. However, previous contributions on SW have not focused on optimizing the communication fabric to improve reliability wireless interface [12]. We propose a highly reliable SW communication fabric along with an efficient transducer interface that is able to match the signal integrity of short range wired NoCs. In summary, in this paper:

1) We propose a realistic wireless channel model to evaluate the losses in emerging WiNoCs. Considering both line-of-sight and reflective transmission in traditional WiNoCs an on-chip reflection channel model which accounts for the transmission medium and built-in material of a practical chip is developed. Experimental analysis of the proposed realistic channel model reveals that, the performance degradation due to separation distance between on-chip antennas is higher with low reliability compared to a conventional channel, modeled over free space.

2) We improve the overall reliability of hybrid wired-wireless Networks-on-Chip on a commercial PCB substrate (Taconic RF-43 [13]). The substrate is basically a thin metal layer coated with low cost dielectric material to support the generated surface wave signals as the reliable wireless communication medium. Additionally, we evaluate the performance of a carefully designed transducer for on-chip wireless communications.

3) We present the design considerations for the realization of the proposed SW fabric as an alternative

communication fabric for the wireless layer of WiNoCs. Depending on the selected parameters of the surface wave communication fabric, evaluated results show that a wide-band 5 dB operational bandwidth of about 40 to 60 GHz can be achieved around 60 GHz operational frequency.

4) We perform cycle-accurate based evaluations of the proposed communication fabric and comparing with emerging WiNoCs as well as conventional reliable wireline communication fabric. Even without any complex error recovery scheme, arbitration or retransmission protocol, the proposed communication fabric can improve the maximum sustainable load of existing WiNoCs and wireline NoCs by an average of 20.9 and 133.3 percent, respectively, with much lower average packet latency.

The rest of the paper is organized as follows. In Section 2, we present the stat-of-the-art contributions on WiNoCs. Section 3 evaluates the reliability of existing wireless communication fabrics for WiNoCs by proposing a realistic channel model. Section 4 presents an reliable WiNoC architecture and formulates the problem of implementing a reliable wireless communication fabric for WiNoCs. Section 5 presents an improved wireless communication fabric for WiNoCs. Section 6 evaluates the transmission strength of the proposed wireless communication fabric. Experimental results in Section 7 validates the performance efficiency of the proposed communication fabric. Finally, the main findings are concluded in Section 8.

2 RELATED WORK

Advances in current integration technology makes it possible to implement a wireless transceiver on a silicon die [14]. Hence, several work have been presented in literature to exploit the energy and performance efficiency of long ranged wireless links in the form of mm-wave over the traditional wire-based NoCs [15]. To improve the throughput and power efficiency of both localized and global data transmission hybrid wired-wireless NoCs have already proposed.

One of the key problems with WiNoCs identified in [6] is the transmission reliability of the wireless channel. As an effort to address this issue, Ganguly et al. [1] proposed an error-control-coding for WiNoCs. By implementing a joint crosstalk triple error correction and simultaneous quadruple error detection codes in the wire line links and Hamming code based product codes in the wireless links with Carbon Nanotube (CNT) antennas, it was demonstrated that, the reliability of the wireless channel could be improved. Similarly, ECC has been adapted in [15] to improve the reliability of WiNoCs. However, ECC introduces timing, area and packet overheads which affects the overall transmission efficiency of the WiNoC [4]. Alternatively, Lee et al. [4] adopted an overhearing scheme for WiNoCs. Here a zero-signaling-overhearing-and-retransmission is presented to manage the packet loss along the wireless channel. A checksum-based error-detection and retransmission scheme at the last hop. Vijayakumaran et al. [16] presented an improved filter design to enhance the performance as well as reduce the error probability of incurred by synchronization delays in CDMA based WiNoCs. However, these techniques rely on the underlying
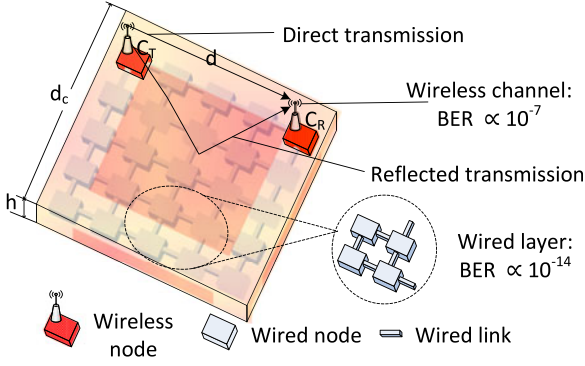
Fig. 1. System model of the communication between two cores in existing hybrid wired-wireless Network-on-Chip.

lossy wireless communication fabric for retransmission of handshake signals, erroneous and non-erroneous packets.

Surface wave interconnect is an emerging wireless communication fabric that has been demonstrated to be power efficient and with high data throughput for on-chip communication [12]. Previous contributions on SW have focused network architecture and performance with considerations of arbitration, packet routing and efficient handling of multicast packets [12]. However, optimizing the communication fabric to improve reliability wireless interface which is a major issue in WiNoCs have not received much attention. We propose a highly reliable SW communication fabric along with an efficient transducer interface that is able to match the signal integrity of short range wired NoCs. In this paper, we propose a reliable 2-D communication fabric to alleviate the these problems. Our aim is to optimize the emerging 2-D communication fabrics to achieve stronger wireless transmission signal in order to improve the reliability of the wireless interface.

3 ON THE RELIABILITY OF EXISTING WIRELESS COMMUNICATION FABRIC FOR NOCS

In order to understand the reduction in performance of WiNoCs due to the reliability issues of wireless channel, it is important to characterize the traditional free-space transmission channel for on-chip wireless communication. Among the key challenges of the channel modeling for WiNoC presented in [17], it is emphasized that no comprehensive work on on-chip channel modeling has been reported. Therefore, considering the deployment of antennas operating in the GHz band in the practical chip, the first contribution of the paper is to investigate the effects of various propagation environment parameters inside a chip package on the performance of WiNoCs. Consequently, a wireless channel model is proposed (by considering the physical characteristics of the transmission medium) to analyse the transmission loss components in order to evaluate the reliability of the state-of-the-art wireless communication fabrics for NoCs.

Fig. 1 illustrates a typical WiNoC architecture where two cores $\mathcal{C}_T$ and $\mathcal{C}_R$ the transmitter and receiver cores, respectively, communicate via millimeter wave channel. Here, we consider a metal cube enclosure as the package with a longest rectangular side of d_C and a height of $h \ll d_C$. Let h_T and h_R denote the height of the mm-Wave antennas (zigzag antennas) at $\mathcal{C}_T$ and $\mathcal{C}_R$, respectively. The material property of the transmission medium between $\mathcal{C}_T$ and $\mathcal{C}_R$ is assumed

to be time-invariant over the transmission of a data frame and changes independently from one frame to another.[1] Let d denote the distance of separation between $\mathcal{C}_T$ and $\mathcal{C}_R$. Accounting for chip floor planning and hence in order to avoid the placement of the cores on/near the edges of the package, d should be less than $d_{\max} = d_C\sqrt{2}$. To accurately model the wireless channel interface of existing WiNoCs, the absorption and resonance of the medium compositions within the chip package should be taken into account, especially in the high frequency band of modern multi-core design. Specifically, various molecules and their isotopologues may cause molecular absorption attenuation (MAA) at various frequency bands [18]. Therefore, the signal transmission between $\mathcal{C}_T$ and $\mathcal{C}_R$ in Fig. 1 suffers from the path loss caused by not only the free-space spreading loss (FSSL) but also the MAA.

For convenience, the main notation and the well-known constants used in this paper are listed in Tables 1 and 2, respectively.

We evaluate the wireless communication fabric for existing wireless Network-on-Chip. Unlike the conventional channel models for the macro-world, on-chip communication introduces new constraints and challenges. Hence in order to study the effect of the wireless channel on the performance of on-chip communication, we propose a channel model that considers the physical dynamics of nanocommunication. In the proposed channel model, the total path loss of electromagnetic signal transmission from $\mathcal{C}_T$ to $\mathcal{C}_R$ within the chip package consists of FSSL and MAA.

3.1 Free-Space Spreading Loss

It can be observed in Fig. 1 that the data transmission between two cores can be carried out via both direct line-of-sight (LoS) and reflected transmission. Therefore, in this paper, we develop a two-ray within-package reflection mode mm-Wave NoCs where the total received E-field $E_T(d, f)$ [V/m] at $\mathcal{C}_R$ consists of the LoS component $E_L(d, f)$ [V/m] and the reflected component $E_R(d, f)$ [V/m]. Summing up these two components, we have

$$
\begin{aligned}
|E_T(d, f)| &= |E_L(d, f) + E_R(d, f)| \\
&= 2\frac{E_0 d_0}{d}\sin\left(\frac{\theta(d, f)}{2}\right),
\end{aligned} \tag{2}
$$

where E_0 [V/m] is the free-space E-field at a reference distance d_0 [m] and $\theta(d, f)$ [rad] is the phase difference between the two E-field components. Here, $\theta(d, f)$ can be approximated by [20]

$$
\theta(d, f) \approx \frac{4\pi h_T h_R f}{\zeta_L d}, \tag{3}
$$

where h_T [m] and h_R [m] denote the height of the antennas at $\mathcal{C}_T$ and $\mathcal{C}_R$, respectively, and $\zeta_L = 2.9979 \times 10^8$ m/s is the speed of light in the vacuum.

From (2) and (3), the received power $P_R(d, f)$ [W] at $\mathcal{C}_R$ can be computed by

---

1. Note that there are various molecules of the gas within the material substance which may change over time. For simplicity, we consider quasi-static channel model in this work.

TABLE 1
Summary of Notation

Notation	Meaning
d [m]	distance between two mm-Wave antennas
d_C [m]	longest rectangular side of the chip package
d_0 [m]	reference distance
h [m]	height of the chip package
h_T, h_R [m]	elevation of the mm-Wave antennas at $\mathcal{C}_T$, $\mathcal{C}_R$, respectively
f [Hz]	transmission frequency
B [Hz]	channel bandwidth
p [atm]	ambient pressure applied on chip
$p_0 = 1$ atm	reference pressure
T_S [K]	system electronic noise temperature
T_M [K]	molecular absorption noise temperature
T' [K]	other noise source temperature
$T_p = 273.15$ K	temperature at standard pressure
$T_0 = 296$ K	reference temperature
L_s, L_a, L	FSSL, MAA, total path loss, respectively
E_L, E_R [V/m]	line-of-sight, reflected components of E-field
E_0, E_T [V/m]	free-space, total received E-field
θ [rad]	phase difference between E_L and E_R
P_T, P_R [W]	transmitted power, received power
G_T, G_R	transmitter antenna gain, receiver antenna gain
τ	transmittance of a medium
κ	medium absorption coefficient
(i, g)	isotopologue i of gas g
$\kappa^{(i,g)}$	individual absorption coefficient of (i, g)
$Q^{(i,g)}$ [mol/m^3]	molecular volumetric density of (i, g)
$\varsigma^{(i,g)}$ [m^2/mol]	absorption cross section of (i, g)
$q^{(}(i, g))$ [%]	mixing ratio of (i, g)
$S^{(i,g)}$ [m^{2}Hz/mol]	line density for the absorption of (i, g)
$\xi^{(i,g)}$ [Hz^{-1}]	spectral line shape of (i, g)
$f_c^{(i,g)}$ [Hz]	resonant frequency of (i, g)
$f_{c_0}^{(i,g)}$ [Hz]	resonant frequency of (i, g) at $p_0 = 1$ atm
$v^{(i,g)}$ [Hz^{-1}]	Van Vleck-Weisskopf asymmetric line shape [19]
$\delta^{(i,g)}$ [Hz]	linear pressure shift of (i, g)
$\alpha_L^{(i,g)}$ [Hz]	Lorentz half-width of (i, g) [19]
α_0 [Hz]	broadening coefficient of air
$\beta^{(i,g)}$ [Hz]	broadening coefficient of (i, g)
ω	temperature broadening coefficient

$$P_R(d, f) = \frac{|E_T(d, f)|^2 G_R \zeta_L^2}{480\pi^2 f^2}$$
$$= \frac{E_0^2 d_0^2 \zeta_L^2}{120\pi^2 d^2 f^2} G_R \sin^2\left(\frac{2\pi h_T h_R f}{\zeta_L d}\right), \qquad (4)$$

where G_R denotes the antenna gain at $\mathcal{C}_R$. Note that the equivalent isotropically radiated power (EIRP) is given by

$$\text{EIRP} = P_T G_T = \frac{E_0^2 d_0^2 4\pi}{120\pi} = \frac{E_0^2 d_0^2}{30}, \qquad (5)$$

where P_T [W] and G_T denote the transmitted power and gain of the mm-Wave antenna at $\mathcal{C}_T$, respectively. From (4) and (5), P_R can be given by

$$P_R(d, f) = \frac{P_T G_T G_R}{\left(\frac{2\pi d f}{\zeta_L}\right)^2} \sin^2\left(\frac{2\pi h_T h_R f}{\zeta_L d}\right). \qquad (6)$$

TABLE 2
List of Constants

Constant name	Symbol	Value
Avogadro constant	ζ_A	6.0221×10^{23} mol^{-1}
Boltzmann constant	ζ_B	1.3806×10^{-23} J/K
Gas constant	ζ_G	8.2051×10^{-5} m^{3}atm/K/mol
Light speed constant	ζ_L	2.9979×10^8 m/s
Planck constant	ζ_P	6.6262×10^{-34} Js

Therefore, the FSSL between $\mathcal{C}_T$ and $\mathcal{C}_R$ (i.e., $L_s(f, d)$) is obtained by

$$L_s(f, d) = \left(\frac{2\pi d f}{\zeta_L}\right)^2 \frac{1}{G_T G_R} \csc^2\left(\frac{2\pi h_T h_R f}{\zeta_L d}\right). \qquad (7)$$

3.2 Molecular Absorption Attenuation

The transmission of electromagnetic waves at frequency f through a transmission medium of distance d introduces MAA due to various molecules within the material substance. Applying Beer-Lambert's law to atmospheric measurements, the MAA of the data transmission from $\mathcal{C}_T$ to $\mathcal{C}_R$ (i.e., $L_a(f, d)$) can be determined by

$$L_a(f, d) = \frac{1}{\tau(f, d)} = e^{\kappa(f)d}, \qquad (8)$$

where $\tau(f, d)$ and $\kappa(f)$ [m^{-1}] are the transmittance and absorption coefficient of the medium, respectively. Here, $\kappa(f)$ depends on the composition of the medium (i.e., particular mixture of molecules along the channel) and it is given by

$$\kappa(f) = \sum_{i,g} \kappa^{(i,g)}(f), \qquad (9)$$

where $\kappa^{(i,g)}(f)$ [m^{-1}] denotes the individual absorption coefficient for the isotopologue i of gas g. For simplicity in representation, the isotopologue i of gas g is hereafter denoted by (i, g).

Applying radiative transfer theory [21], $\kappa^{(i,g)}(f)$ can be determined by

$$\kappa^{(i,g)}(f) = \frac{p}{p_0} \frac{T_p}{T_S} Q^{(i,g)} \varsigma^{(i,g)}(f), \qquad (10)$$

where p [atm] is the ambient pressure applied on the designed SoC, T_S [K] is the system electronic noise temperature, $p_0 = 1$ atm is the reference pressure, $T_p = 273.15$ K is the temperature at standard pressure, $Q^{(i,g)}$ [mol/m^3] is the molecular volumetric density (i.e., number of molecules per volume unit of (i, g)) and $\varsigma^{(i,g)}(f)$ [m^2/mol] is the absorption cross section of (i, g). Here, $Q^{(i,g)}$ is obtained by the Ideal Gas Law as

$$Q^{(i,g)} = \frac{p}{\zeta_G T_S} q^{(i,g)} \zeta_A, \qquad (11)$$

where $\zeta_G = 8.2051 * 10^{-5}$ m^{3}atm/K/mol is the Gas constant, $\zeta_A = 6.0221 \times 10^{23}$ mol^{-1} is the Avogadro constant and $q^{(i,g)}$ [percent] is the mixing ratio of (i, g).

In (10), $\varsigma^{(i,g)}(f)$ is given by

$$\varsigma^{(i,g)(f)} = S^{(i,g)}\xi^{(i,g)}(f), \tag{12}$$

where $S^{(i,g)}$ [m^{2}Hz/mol] is the line density for the absorption of (i,g) (i.e., the absorption peak amplitude of (i,g)) and $\xi^{(i,g)}(f)$ [Hz^{-1}] is spectral line shape of (i,g) determined by

$$\xi^{(i,g)}(f) = \frac{f}{f_c^{(i,g)}} \frac{\tanh\left(\frac{\zeta_P \zeta_L f}{2\zeta_B T_S}\right)}{\tanh\left(\frac{\zeta_P f_c^{(i,g)}}{2\zeta_B T_S}\right)} \upsilon^{(i,g)}(f), \tag{13}$$

where $f_c^{(i,g)}$ [Hz] is the resonant frequency of (i,g), $\zeta_P = 6.6262 \times 10^{-34}$ Js is the Planck constant, $\zeta_B = 1.3806 \times 10^{-23}$ J/K is the Boltzmann constant and $\upsilon^{(i,g)}(f)$ [Hz^{-1}] is the Van Vleck-Weisskopf asymmetric line shape of (i,g). In (13),

$$f_c^{(i,g)} = f_{c_0}^{(i,g)} + \delta^{(i,g)} \frac{p}{p_0}, \tag{14}$$

where $f_{c_0}^{(i,g)}$ [Hz] is the resonant frequency of (i,g) at reference pressure $p_0 = 1$ atm and $\delta^{(i,g)}$ [Hz] is the linear pressure shift of (i,g). Also, the Van Vleck-Weisskopf asymmetric line shape of (i,g) in (13) is given by

$$\upsilon^{(i,g)}(f) = 100\zeta_L \frac{\alpha_L^{(i,g)}}{\pi} \frac{f}{f_c^{(i,g)}} \left[\frac{1}{(f - f_c^{(i,g)})^2 + (\alpha_L^{(i,g)})^2} + \frac{1}{(f + f_c^{(i,g)})^2 + (\alpha_L^{(i,g)})^2} \right], \tag{15}$$

where $\alpha_L^{(i,g)}$ [Hz] is the Lorentz half-width of (i,g). Here, $\alpha_L^{(i,g)}$ is computed by

$$\alpha_L^{(i,g)} = \left[(1 - q^{(i,g)})\alpha_0 + q^{(i,g)}\beta^{(i,g)} \right] \frac{p}{p_0} \left(\frac{T_0}{T_S} \right)^\omega, \tag{16}$$

where α_0 [Hz] is the broadening coefficient of air, $\beta^{(i,g)}$ [Hz] is the broadening coefficient of (i,g), $T_0 = 296$ K is the reference temperature and ω is the temperature broadening coefficient. Let $L(f,d)$ denote the total path loss for signal transmission at frequency f [Hz] over distance d [m]. From (7), (8) and (9), the total path loss of the proposed channel model is

$$L(f,d) = L_s(f,d)L_a(f,d)$$
$$= \left(\frac{2\pi df}{\zeta_L} \right)^2 \frac{1}{G_T G_R} \csc^2 \left(\frac{2\pi h_T h_R f}{\zeta_L d} \right) \prod_{i,g} e^{\kappa^{(i,g)}(f)d}. \tag{17}$$

Remark 1 (Effectiveness of the proposed channel model). In (17), it can be shown that $\kappa^{(i,g)} \geqslant 0 \ \forall i,g$. This means the proposed channel model always has a higher total path loss than the conventional channel model with no MAA, and thus can represent the practical scenario as a performance benchmark.

Remark 2 (Environment-aware channel model). The proposed channel model depends on not only the distance between two cores $\mathcal{C}_T$ and $\mathcal{C}_R$ but also the absorption of gas molecules, the temperature and the ambient

pressure applied on the chip. In fact, from (10) - (16), the individual absorption coefficient for the isotopologue i of gas g (i.e., $\kappa^{(i,g)}(f)$) is shown to be dependent but not monotonically varied over the frequency.

3.3 Channel Capacity of WiNoCs

We analyze the channel capacity of the wireless channel of WiNoCs with respect to the proposed channel model where the following observations could be made[2]:

Lemma 1. *The channel capacity in bits/s of a nanocommunication system between two on-chip antennas is obtained by*

$$C(P_T, d) = \sum_{k=1}^{K} \Delta f \log_2 \left[1 + \frac{P_T G_T G_R \sin^2\left(\frac{2\pi h_T h_R f_k}{\zeta_L d}\right)}{\zeta_B \left(\frac{2\pi d f_k}{\zeta_L}\right)^2 \Delta f} \right.$$
$$\left. \times \frac{1}{(T_S + T_0)\prod_{i,g} e^{\kappa^{(i,g)}(f_k)d} - T_0} \right], \tag{18}$$

where K is the number of sub-bands in the total channel bandwidth of B [Hz], $\Delta f = B/K$ [Hz] is the width of each sub-band and f_k [Hz] is the center frequency of the kth sub-band.

Proof. As the signal-to-noise ratio (SNR) is required for evaluating the achievable capacity of a communications system, we first derive the total noise power of the nanocommunications between two mm-Wave antennas. At frequency f [Hz], the total noise temperature at $\mathcal{C}_R$ located at d [m] from $\mathcal{C}_T$ (i.e., $T_{tot}(f,d)$ [K]) consists of the system electronic noise temperature (i.e., T_S [K]), the molecular absorption noise temperature (i.e., $T_M(f,d)$ [K]) and other noise source temperature (i.e., T' [K]), i.e.,

$$T_{tot}(f,d) = T_S + T_M(f,d) + T'. \tag{19}$$

Assuming that $T_S + T_M(f,d) \gg T' \ \forall f,d$, we have

$$T_{tot}(f,d) \approx T_S + T_M(f,d). \tag{20}$$

Here, $T_M(f,d)$ is caused by the molecules within transmission medium, and thus can be expressed via the transmittance of the medium as

$$T_M(f,d) = T_0(1 - \tau(f,d)) = T_0 \left(1 - \prod_{i,g} e^{-\kappa^{(i,g)}(f)d} \right). \tag{21}$$

Substituting (21) into (20), we obtain

$$T_{tot}(f,d) \approx T_S + T_0 \left(1 - \prod_{i,g} e^{-\kappa^{(i,g)}(f)d} \right). \tag{22}$$

The total noise power at $\mathcal{C}_R$ given transmission bandwidth B is therefore given by

---

2. The channel capacity is measured as the maximum achievable rate at which the information can be reliably transmitted over the communication channel between two wireless cores. The BER can be derived accordingly given the signal-to-noise ratio (SNR) at the receive antenna when considering both FSSL and MAA in the channel modelling. Although the BER performance is worth a detailed evaluation, it is beyond the scope of this work.

$$P_N(d) = \zeta_B \int_B T_{tot}(f, d) df. \qquad (23)$$

Note that the wireless channel for on-chip communication is highly frequency-selective and the molecular absorption noise is non-white. Therefore, we can divide the total bandwidth B into K narrow sub-bands to evaluate the capacity, in bits/s, as follows:

$$C(P_T, d) = \sum_{k=1}^{K} \Delta f \log_2 \left[1 + \frac{P_T}{\zeta_B L(f_k, d) T_{tot}(f_k, d) \Delta f} \right], \qquad (24)$$

where Δf is the width of sub-band and f_k is the center frequency of the kth sub-band. Substituting (17) and (22) into (24), we obtain (18) and thus proving the above lemma. □

Corollary 1. *When $h_T \ll d$, $h_R \ll d$, $d \to 0$ and $G_T = G_R = 1$, the channel capacity of a nanocommunication system can be given by*

$$C(P_T, d) \approx \sum_{k=1}^{K} \Delta f \log_2 \left[1 + \frac{P_T h_T^2 h_R^2}{\zeta_B d^4 \Delta f} \right.$$
$$\left. \times \frac{1}{T_S + (T_S + T_0)\kappa(f_k)d} \right]. \qquad (25)$$

Proof. As $h_T \ll d$, $h_R \ll d$ and $d \to 0$, applying Maclaurin series [22, eq. (0.318.2)], it can be approximated that

$$\sin^2 \left(\frac{2\pi h_T h_R f_k}{\zeta_L d} \right) \approx \left(\frac{2\pi h_T h_R f_k}{\zeta_L d} \right)^2, \qquad (26)$$

$$\prod_{i,g} e^{\kappa^{(i,g)}(f_k)d} \approx 1 + \sum_{i,g} \kappa^{(i,g)}(f_k)d = 1 + \kappa(f_k)d. \qquad (27)$$

Substituting (26) and (27) into (18) with the assumption of $G_T = G_R = 1$, the corollary is proved. □

It can be deduced from the above realistic on-chip free space wireless channel model that, the total path loss of electromagnetic signal transmission between a transmitting and receiving pair has both FSSL and MAA components which drastically reduce the performance and reliability of WiNoCs as will be shown latter in Section 7. Consequently, it is crucial to explore alternative communication fabric that is able transmit wireless signals with minimum loss. Therefore, as a second contribution, this work presents a novel CMoS compatible communication fabric for on-Chip networks which is able to mitigate the reliability issues of the wireless channel as detailed in the remaining sections of the paper.

4 RELIABLE WIRELESS NoCs

4.1 Network Architecture

A promising way to mitigate the communication overhead incurred by the multi-hop channels among remote cores in traditional wireline NoCs is to adopt wireless communication fabric as a supplementary material. Surface wave communication has been recently demonstrated as a feasible on-chip wireless solution with improved long-range communication, low-power and high bandwidth [12]. Here,
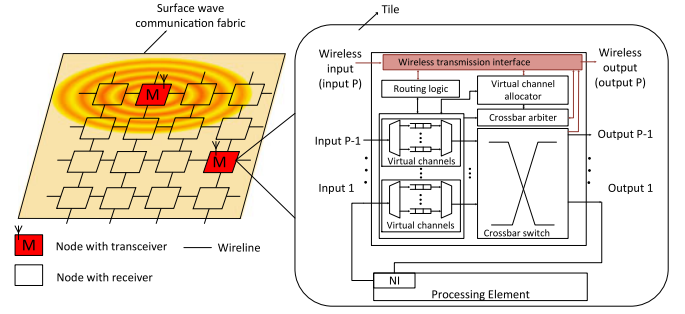

Fig. 2. Hybrid wireline-surface wave NoC architecture.

the wireless communication layer of WiNoCs is replaced with a waveguide medium as the surface wave communication fabric for global communication which generates a NoC architecture as shown in Fig. 2.

The 2-D guided wave enhances low power-fast global communication which gives reasonably high performance to area ratio with an E-field decay rate of

$$E_{decay} \propto \frac{1}{\sqrt{(d)}}. \qquad (28)$$

Compared to traditional mm-Wave-based WiNoCs, the hybrid wired-SW NoC architecture has significantly reduced power consumption due to the propagation of wireless signal in a 2-D guided medium.

To adapt to the wireless channels, the routers at the wireless nodes in WiNoCs are equipped with a wireless transmission interface which serves as a bridge between the wireless and the wireline communication layers. The wireless transmission interface, responsible for transmitting and receiving wireless signals, works closely with the routing logic, virtual channel allocator, arbiter and crossbar switch for efficient wireless signal transmission. Hence, an unreliable wireless communication fabric with numerous erroneous signal transmissions will increase the competition among the wireline and wireless data for these shared resources.

As an effort to increase the reliability of such networks, the wireless transmission interface can be equipped with a retransmission buffer and a suitable error encoding and decoding scheme. However, the overhead of the erroneous packets as well as the retransmission process introduces contention on the wireless as well as the wireline layers, and hence have drastic effects on the performance of the WiNoC. Moreover, buffer spaces contribute significantly to the total power consumption of the NoC [23] and should be used judiciously.

In the following sections we present the design considerations for the proposed reliable wireless communication fabric in the form of surface wave.

4.2 Problem Formulation

Lemma 2. *For Transverse Magnetic mode (TM)-surface wave propagation in a 2-D on-chip communication fabric, a dielectric coated conductor with sufficiently high inductive reactance X_s is required.*

Proof. The TM signal independent of the y coordinate that propagates along the x axis and satisfies the Maxwell equations [24] is evaluated.
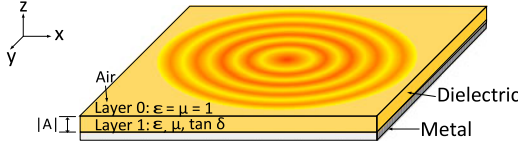
Fig. 3. 2-D waveguide sheet implemented with a dielectric layer (with a loss tangent $tan\,\delta$) placed over a perfectly conducting plane.

Fig. 4. Interface between the 2-D guided wave channel and the wireline channel.

In free space, *Layer 0* ($\epsilon = \mu = 1$), the following can be derived:

$$H_y = e^{jk_1}(z - |A|)e^{j(\beta x)} \tag{29}$$

$$E_z = -\frac{Z_0 \beta}{k_0 \epsilon} e^{jk_1}(z - |A|)e^{j(\beta x)} \tag{30}$$

$$E_x = \frac{Z_0 k_1}{k_0 \epsilon} e^{jk_1}(z - |A|)e^{j(\beta x)}, \tag{31}$$

where k_0 and Z_0 are the number of waves and the impedance of free space, respectively. β is the propagation constant. Inside the dielectric layer, *Layer 1*, the electric and magnetic field components are given by

$$H_y = \frac{\cos(k_2 z)}{\cos(k_2 |A|)} e^{j(\beta x)} \tag{32}$$

$$E_z = -\frac{\beta \cos(k_2 z)}{Z_0 k_0 \epsilon \cos(k_2 |A|)} e^{j(\beta x)} \tag{33}$$

$$E_x = j\frac{Z_0 k_2 \sin(k_2 z)}{k_0 \epsilon \cos(k_2 |A|)} e^{j(\beta x)}, \tag{34}$$

where k_1 and k_2 are the transverse waves numbers in Layer 0 and Layer 1, respectively, which can be solved through the Helholtz wave equation [24]

$$K_1 = \sqrt{k_0^2 - \beta^2} \tag{35}$$

$$K_1 = \sqrt{k_0^2 \epsilon \mu - \beta^2}. \tag{36}$$

The surface impedance Z_s of the interface between Layer 0 and Layer 1 is given by

$$Z_s = -\frac{E_x}{H_y} = -Z_0 \frac{k_1}{k_0}. \tag{37}$$

To enable the field concentration in Layer 0 nearer to the surface of Layer 1 for TM-surface wave propagation, Z_s must be inductive. Thus the imaginary part of k_1 should be positive. Therefore to design a 2-D waveguide fabric for on-chip communication, a dielectric coated conductor with sufficiently high inductive reactance X_s needs to be implemented.

The surface reactance X_s for TM surface wave transmission in is given by

$$X_s = 2\pi f \mu_0 \left[\frac{\epsilon - 1}{\epsilon} |A| + 0.5\Delta \right]. \tag{38}$$

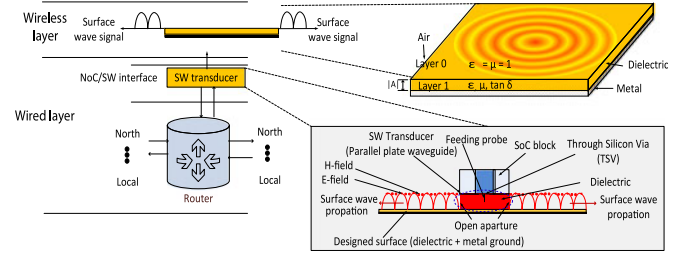Eq. 38 confirms that the realization of TM mode for 2-D wave propagation for communication is related to the operating frequency, f, dielectric constant, ϵ, thickness of the dielectric material, $|A|$, and the skin depth of the metal conductor, Δ. The skin depth is given by

$$\Delta = \sqrt{\frac{1}{\pi f \mu_0 \sigma}}, \tag{39}$$

where σ is the conductivity of the metal conductor.   □

Lemma 2 shows how surface impedance can be evaluated from the fundamental parameters, the E-field and H-field on the reactive surface. Moreover, our recently published work in [25] reveals that S_{21}, which represents the signal strength transferred from the transducer Tx to the receiver Rx, can be maximized by the appropriate value of surface impedance Z_s. Hence to solve the problem of improving the reliability of the wireless channel of emerging WiNoCs, our objective is to determine the particular design parameters of the TM surface wave communication medium with a positive surface reactance along with a transducer to operate at a frequency f such that:

$$\max_{\forall Tx \rightarrow Rx \in T} (S_{21}), \tag{40}$$

subject to:

$$\psi = BER_w - BER_T, \tag{41}$$

where

$$\psi \leq min, \tag{42}$$

where T is the set of transducers with transmitters and/or receivers, respectively. BER_w and BER_T are the bit error rates of the wireline and wireless channels, respectively. The most reliable design has a $\psi = 0$ and hence the minimum (min in Eq. 42) must be as close to zero as possible.

5 AN IMPROVED WIRELESS COMMUNICATION FABRIC FOR EMERGING WIRELESS NOC ARCHITECTURES

Surface wave wireless communication medium can be implemented with a thin lossy dielectric coated conductor plane surrounded by free space. Our aim is to design a communication medium with minimum transmission loss as possible in order to improve the reliability of WiNoCs. Fig. 4 shows the functional blocks of the proposed surface wave communication fabric for WiNoC. Here, a dielectric coated metal layer is employed as a guided medium for surface wave signal propagation. With the right design consideration, the transducer

and wireless medium could be designed to transmit with minimum communication loss and achieve a transmission reliability similar to the wireline communication layer.[3] To generate an efficient TM surface wave signal, the following considerations are made for the design of the 2-D waveguide sheet. We use commercially available Taconic $RF - 43$ material. Hence, we employ a low loss and cost-effective TacLam-plus material which is laser ablatable, non-reinforced microwave substrate that is ideal for very low loss substrate [13] with 0.2 mm thickness as the dielectric (Layer 1 in Fig. 4).[4] For the same frequency, it can be deduced from Eq. 38 that X_s will increase with $|A|$. Therefore, more wave will stay on the surface and in effect increase the efficiency. However, for TM surface propagation, X_s cannot be too high, otherwise the wave will propagate into the dielectric instead of at the boundary of the air-dielectric surface. Hence, by introducing the 0.25 mm thick Taconic material, we can achieve a surface reactance X_s of 30Ω to 150Ω over the wide frequency range of 20 GHz to 100 GHz for TM mode surface wave. To achieve a high surface wave efficiency, a thin substrate is employed. Our goal is to improve the gain between the transmitted signal and the received signal. Hence, we investigate the design of an efficient transducer that is able to translate between wireline and wireless signals at the preferred operating frequency (60 GHz in this paper). The designed transducer consists of a parallel waveguide fed by an optimized probe through an open aperture. The transducer is coupled to a transceiver circuit which is responsible for modulation, signal transmission and receiving capabilities.

For a reliable transmission, a low power consumption transceiver circuit which has a wide bandwidth with high data throughput must be considered. Hence, we adopt the low-power non-coherent on-off keying (OOK) modulator for our implementation. Embedded in the transmitter design is an up-conversion mixer and a power amplifier (PA) while the receiver is equipped with a low noise amplifier (LNA), a baseband amplifier and a down-conversion mixer. A single injection-lock voltage-controlled oscillator (VCO) is used for both the transmitter and the receiver to reduce the area overhead and power consumption. More details on the implementation of the transceiver module along with the circuitry can be found in [5].

At the nodes equipped with both wireless transmission and receiving capabilities, a CMOS-based circulator is employed as a communication bridge between the transmitter, receiver and the 2-D waveguide medium, to enable the use of a single wave feeder at the nodes [26]. It should be noted that some nodes in the WiNoCs do not have transmitting capabilities and hence are only equipped with the receiver circuits. The OOK transceiver is able to achieve a BER less than 10^{-14} and at data rate of at least 16 Gb/s for
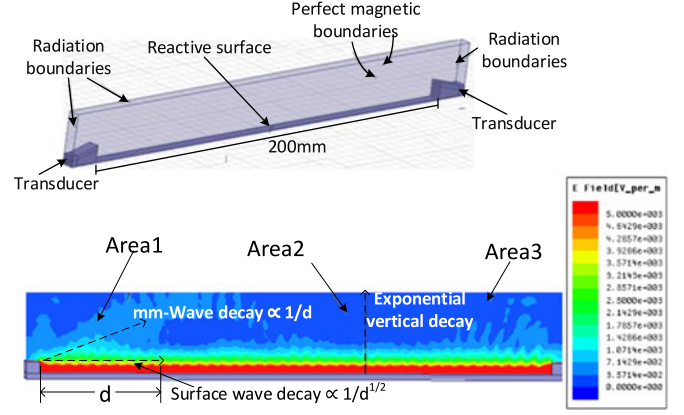

Fig. 5. 2D simulation model for surface wave communication system.

the designed communication range of 20 mm which is comparable to that of the traditional wireline network. Hence in this paper we adopt the above transceiver [5].

Hence, the challenge is to demonstrate that the receive signal power at the destination node is similar to the transmit signal power at the source node over the proposed wireless communication fabric, which is demonstrated in the next section.

6   EVALUATION OF PROPOSED WIRELESS COMMUNICATION FABRIC

To demonstrate the effectiveness of the proposed wireless communication fabric, we have performed simulations in Ansys High Frequency Structured Simulator [27]. Fig. 5 shows the HFSS simulation setup. The transducers are placed as far as 200 mm (equivalent to 40 free space wavelengths at operating frequency of 60 GHz) apart to investigate the signal integrity and the possible performance benefits of the proposed 2D waveguide over existing on-chip wireless NoCs. For comparisons, we have also implemented a model of mm-Wave for on-chip communication. Here, a zigzag antennas which is considered to be the most efficient antenna for mm-Wave on-chip communication is employed. The zigzag antennas are separated by a distance of only 20 mm.

As shown in Fig. 5, when the transducers and the surface wave sheet are properly designed, the electric field distribution is concentrated in Area2 which demonstrates that a high percentage of the transmitted signal is successfully launched into the surface. Across the long distance separation between of 200 mm (from Area1 to Area3) the transducer and transceiver, a near constant electric field distribution is achieved. Also the electric field decays exponentially away from the implemented surface, indicating that surface wave is successfully launched and received with a high signal efficiency.

Fig. 6 compares the S_{21} (dB) of different technologies. It can be seen that, the reactive surface appears to have a flat response over a wide frequency range and having a 3 dB bandwidth of almost 45 GHz (from 35 to 80 GHz with $tan\,\delta = 0.01$), and a 5 dB bandwidth of almost 60 GHz (from 30 to 87 GHz with $tan\,\delta = 0.01$). On the other hand, Fig. 6 also shows that the S_{21} of mm-Wave is around -36 dB which is significantly lower than that of the proposed communication fabric.

3. With the addition of AC-DC converters the proposed surface wave communication fabric can also be used for on-chip wireless power transmission.

4. Through-Silicon-Via (TSV) is only used internally in the SoC, which sits on top of the surface wave communication fabric (the lowest layer). Due to the difference in thickness between the 2-D waveguide and the height of TSV (about 20 μm), it is recommended that the SoC block and surface transducer are fabricated separately and integrated by flip-chip bonding.
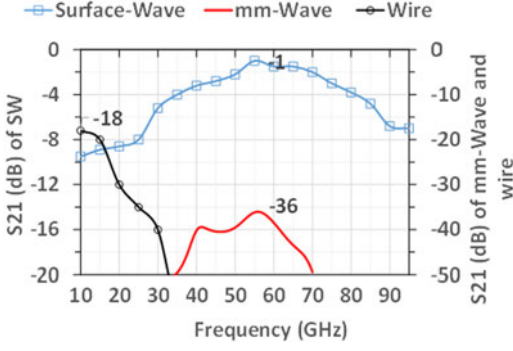
Fig. 6. S_{21} (dB) over wide-band frequency on the reactive surface.

Moreover, though wireline can achieve a high signal strength, transmission frequency high transmission frequency of the wires is inhibited by induced coupling, crosstalk and temperature induced noises [1]. Therefore, the proposed communication fabric is able to successfully excite and transmit high frequency-high bandwidth surface wave signals with high reliability (S_{21} of 0 to -2 dB). Consequently, when employed as the wireless communication medium for hybrid wired-wireless NoCs, the proposed fabric improves the reliability of the NoC with a BER comparable to that of wireline NoCs.

Fig. 7 shows the propagation loss for different transducer designs, assuming zero dielectric loss. It demonstrates that surface wave signal generated with an off-the-shelf transducer (eg., patch antenna) results in a much lower S_{21} (around -84 dB) at the operating frequency (64 GHz). It should be noted that special attention is required to design the transducer to match with the surface impedance X_s in wide frequency band which not realistic for Commercial off-the-shelf (COTS), such as common monopoles or patch antennas.

Fig. 8 shows that, for a fixed signal to noise ratio (SNR) of a communication fabric with an attenuation constant α, the improvement in rate of change in transmission gain $G_{a,dB}$ for a receiver node placed at d' from a transmitting node at d which is given by

$$G_{a,dB} = \frac{-20}{T_{(d'-d),ps}} \left(\log_{10}\left(\frac{d'}{d}\right) + \alpha(d'-d)\log_{10}e \right) \quad (43)$$

of the proposed communication fabric (SW) over mm-Wave increases significantly as the separation between transmitting node and receive node increases. This is because as the
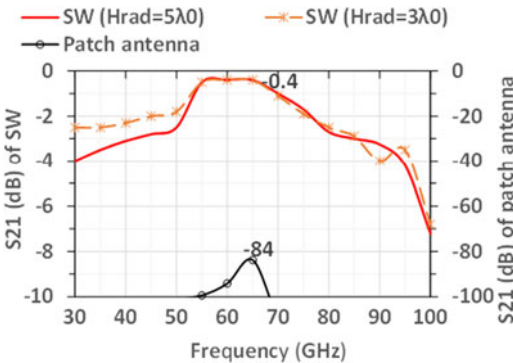

Fig. 7. S_{21} (dB) over wide-band frequency on the reactive surface with different transducer designs.
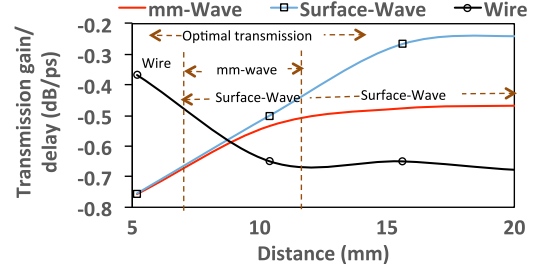

Fig. 8. Variation of ratio of rate of change of transmission gain with distance for different on-chip communication medium.

distance between the communicating pair increases, the E-field of mm-Wave decays at an exponential rate in free space which lowers the signal strength as shown in Fig. 5. In the wireline channels, there is no need for transceiver circuits to convert wireless signals. Hence at low distances, wireline is more efficient than the wireless communication fabric. However, the delay along the wires have drastic effects which causes significant drop in the rate of transmission gain as the distance to destination node increases. Consequently, the proposed communication fabric provides a feasible performance to distance tradeoff with higher transmission gains and lower delays when combined with wires in hybrid WiNoCs.

7 EXPERIMENTAL RESULTS

Cycle-accurate experiments are performed using an extended version of Noxim simulator, an open source SystemC simulator for NoCs. The power of the router is modeled with ORION2.0 NoC power simulator. We adapt the BER and the S_{21} of the communication fabric as the error model. We investigate a wide range of WiNoC configurations with buffer depth of six flits and packet size of three flits. Both regular and non-regular mesh topologies are investigated with a setup as summarized in Table 3. Five nodes in the WiNoC, which are evenly distributed in the NoC, are equipped with transceivers.[5] All other nodes have receivers. We consider both deterministic XY routing and adaptive West-first routing algorithms. In both cases, the underlying routing algorithm is employed in the wireline layer until a wireless node with a transceiver is encountered. Packets are then sent to the destination node via the single-hop wireless channel. In West-first routing technique we employ buffer level selection scheme to avoid creating bottleneck along the wireless channel. In the experiments we compare the effects of the reliability of the proposed surface wave with mm-Wave in WiNoCs and conventional wireline mesh.[6]

Note for a given BER, the packet error ratio which dictates the probability of packet retransmission is given by

$$p_p = 1 - (1 - p_e)^{|P|}, \quad (44)$$

---

5. The number of transceiver nodes is based on the available frequency range for 45 nm, which is estimated to be four channels (in addition to the frequencies specified for control signals). However, this range is scaling with technology. Hence in this paper, five nodes are adopted [12].

6. The proposed wireless communication fabric is compatible with any wireless NoC topology. However for correlation purposes, we have considered 2-D mesh as the baseline NoC topology.

TABLE 3
Simulation Setup

NoC dimensions	$6 \times 4, 5 \times 5, 6 \times 6, 8 \times 8, 10 \times 10$
Virtual channels (VC)	4
NoC buffer (flit depth)	6
Links and NoC buffer width	128 bits
Transceiver nodes	5
FDMA carrier frequencies per node	128
Fixed BER	mm-Wave: 10^{-7}, wire: 10^{-14}, SW: 10^{-13}
Tile dimensions	3.6×5.2 mm^2
Processing element	Two Pentium class IA-32 cores
cache	Two 256 KB private L2 caches

where $|P|$ is the packet length in bits and p_e is the bit error probability which is the expectation value of the BER for the communication fabric. Thus, Eq. 44 is modeled and imported into the NoC simulator to assign the probability of retransmission of different communication fabrics at different packet injection rates.[7] Alternating bit protocol is used for transmitting and receiving data, and credit flit (ACK/NACK). While wormhole flow control is used for the wireline layer, FDMA media access control is adopted to give more than one node the right to transmit over the shared wireless medium at a data rate of 256 Gbps in one clock cycle over 128 carrier frequencies.

7.1 Impact of Communication Fabric on NoCs

We treat the hybrid wired-wireless network as a whole and evaluate the effect of the wireless communication fabric on the average packet latency. It can be observed in Fig. 15 that hybrid wired-surface wave NoC (SW) has less average packet delays and can sustain about 29 percent more traffic load compared to mm-Wave WiNoC under both deterministic and adaptive routing in random traffic pattern. The performance improvement is even more significant (over 100 percent) when SW is compared to conventional wireline network.

To validate these findings, we have applied two transpose synthetic traffic patterns where source nodes generate packets to specific destination nodes. As shown in Fig. 10, SW outperforms mm-Wave WiNoC in all cases. Though no special wireless channel selection method is employed in deterministic XY routing (Figs. 9a, 9c and 10a), the extra traffic load introduced by the high rate of retransmitted erroneous packets causes contention in both the wireline and wireless channels of mm-Wave WiNoCs. On the other hand, though buffer levels are employed for wireless channel selection in west-first adaptive routing (Figs. 9b, 10b, and 10c) the error rate along the wireless channel in mm-Wave is much higher than surface wave channel, hence packets in mm-Wave WiNoC experience longer delays compared to SW.

7. An alternative approach is to inject an erroneous packet after millions of cycles as dictated by the BER which requires extremely large simulation cycles. Experiments conducted with significantly long simulation lengths (which are in order of millions) show that our setup yields similar results (with shorter but reasonable simulation lengths) as the packet error ratio is a directly proportional to the BER.

We investigate the behavior of WiNoCs under a wide range of regular NoC dimensions with five transceiver nodes under random traffic pattern. As shown in Fig. 11a, SW can sustain about 98 percent more traffic compared to mm-Wave WiNoC when the NoC dimensions is increased to 6×6. This is mainly due to the stronger signal strength with minimum BER of the SW channel over mm-Wave when the distance between remote nodes is increased. Consequently, the number of erroneous packets and retransmissions injected into the network in mm-Wave WiNoC due to the lossy wireless channel increases the network contention even under medium traffic conditions. However, the maximum sustainable load of SW drops to about 25 percent more efficient compared to mm-Wave WiNoC when the dimension is increased to 10×10. This is expected as the number of nodes equipped with transceivers is kept constant (five transceiver nodes) in all cases. As evident in the significantly low saturation rate of traditional wireline NoC (Fig. 11) the contention in the wireline layer have more dominant effect on average packet latency as the number of nodes in the network increases over fixed number of wireless nodes. On the average, SW improves the maximum sustainable load by 27.8 and 133.3 percent compared to mm-Wave and wireline, respectively, even when a small number of wireless transmitting nodes are used.

7.2 Realistic Applications

To further validate the performance benefits of the proposed communication fabric, M5 simulator [28] is employed to acquire memory access traces from a full system running PARSEC v2.1 benchmarks [29] which is used to drive our cycle-accurate network simulator. In the setup, 64 two-wide superscalar out-of-order cores with private 32 KB L1 instruction and data caches as well as a shared 16 MB L2 cache are employed. Following the methodology presented in Netrace [30], the memory traces are post-processed to encode the dependencies between transactions. Consequently, the communication dependencies are enforced during the simulation. Memory accesses are interleaved at 4 KB page granularity among four on-chip memory controllers. A summary of the benchmarks is presented in Table 4. Thus we apply a wide range of benchmarks with varied of granularity and parallelism to study the effects of different wireless communication fabrics on WiNoCs. For each trace, we simulate at least 100 million cycles of the PARSEC-defined region of interest (ROI) where we schedule two threads per core.

Fig. 12 shows the average performance improvement of SW over mm-Wave WiNoC and wireline in terms of average packet latency in realistic traffic traces. In all workloads, SW communication fabric can has lower packet latency compared with other on-chip communication fabrics. Particularly, in high contention workload such as swaptions and channeal with large number of packets simulated over a wide simulation cycle the proposed communication fabric achieves over 60 percent improvement in the average packet latency compared to the baseline (wireline) NoC.

Fig. 13 shows that the electric field decay rate (estimated with Eq. 1 and 28) of SW signal is much slower than that of mm-Wave. Particularly, the reduced rate of decay of SW signal compared to mm-Wave signal is consistent with the improvement in power consumption presented in Fig. 14.
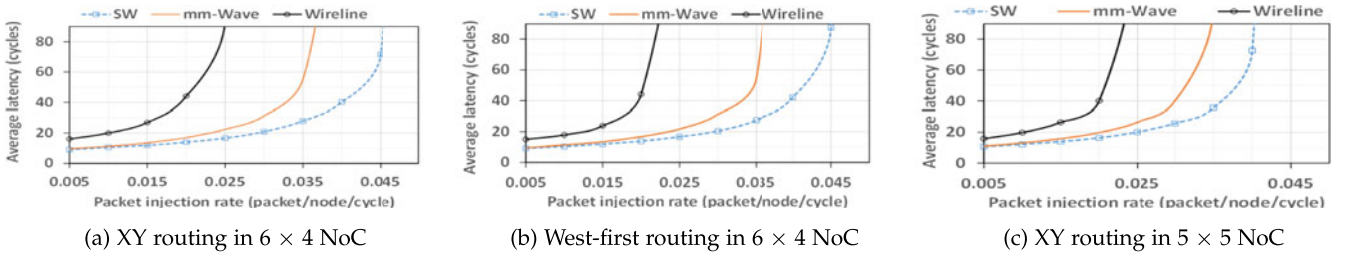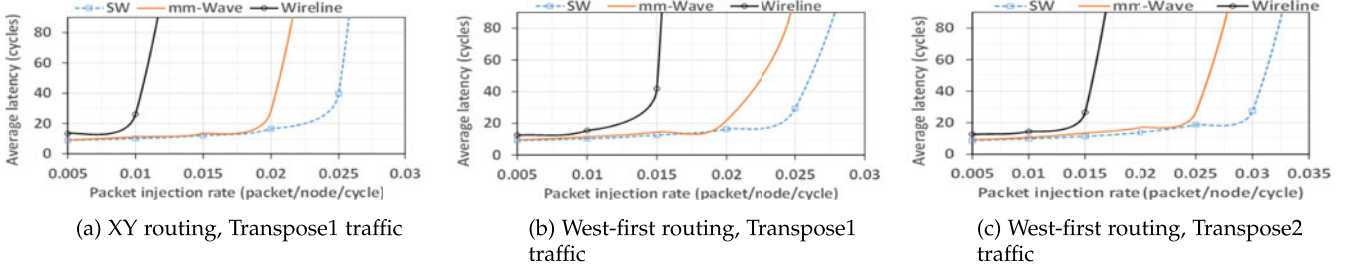
(a) XY routing in 6 × 4 NoC   (b) West-first routing in 6 × 4 NoC   (c) XY routing in 5 × 5 NoC

Fig. 9. Average packet latency under random traffic patterns in 6 × 4 and 5 × 5 NoCs, six buffer per port, four VCs and four transceiver nodes.

(a) XY routing, Transpose1 traffic   (b) West-first routing, Transpose1 traffic   (c) West-first routing, Transpose2 traffic

Fig. 10. Average packet latency under transpose traffic patterns in 6 × 4 NoC, six buffer per port, four VCs and four transceiver nodes.

(a) 6 × 6 NoC   (b) 8 × 8 NoC   (c) 10 × 10 NoC
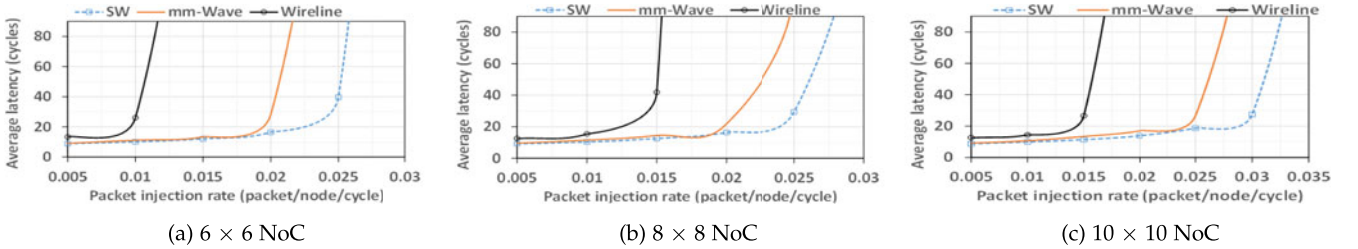
Fig. 11. Average packet latency under different NoC dimensions, 6 buffer per port, four VCs, four transceiver nodes, random traffic and west-first routing.

7.3 Power Consumption

Both static and dynamic power of the router is calculated in Orion2.0 model for 45 nm technology. The wireline links along the x and y dimensions are modeled as 3.6 mm and 5.2 mm, respectively. For the wireless link power analysis along the surface wave and mm-Wave channels, we exploit the S_{21} signal voltage gain between the transmitter and receivers [12]:

$$S_{21} = E + 20 \lg e^{-\alpha d}, \qquad (45)$$

where α is the attenuation constant of the wireless communication fabric, d is the separation between the transmitting and receiving nodes and E is the loss constant due to the transducer. Based on extracted values from a Matlab fitting tool [12] and conducted experiments (see Section 6), α is calculated as 6.33 and E values of -23.8 and -1 are calculated for mm-Wave and surface wave, respectively. For the power consumption of the transceiver 24 mW per sub-channel is used [31]. These values have been imported in to the simulator for power estimation. In general, for high contention workload such as swaptions and channeal with large number of packets simulated an average leakage power and dynamic power of 15 and 35 mW, respectively, was recorded for mm-Wave, while an average of 8.3 mW leakage power and 35 mW leakage power was recorded for WiNoCs with surface wave. Fig. 14 shows the power efficiency of surface wave over mm-Wave in various WiNoC dimensions and under different traffic patterns. For PARSEC benchmark we use medium input set for all traces except swaptions where large input set is adopted. The figure shows that mm-Wave consumes up to 17 percent more power compared to the proposed surface wave fabric when employed as the wireless communication channel for WiNoCs under synthetic traffic patterns. The percentage increase in power savings is even more significant under realistic traffic traces. This is because the mm-Wave channel is lossy with high signal loss constant due to free space propagation while the proposed surface wave communication fabric transmits TM signals with high S_{21}. Particularly, due to reduction in the number of erroneous packets and retransmissions, the SW reduces the

TABLE 4
Simulated PARSEC Traces

Benchmark	Input Set	Cycles	Total Packets
blackscholes	small	255M	5.2M
blackscholes	medium	133M	7.2M
channeal	medium	140M	8.6M
dedup	medium	146M	2.6M
fluidanimate	small	127M	2.1M
fluidanimate	medium	144M	4.6M
swaptions	large	204M	8.8M
vips	medium	147M	0.9M
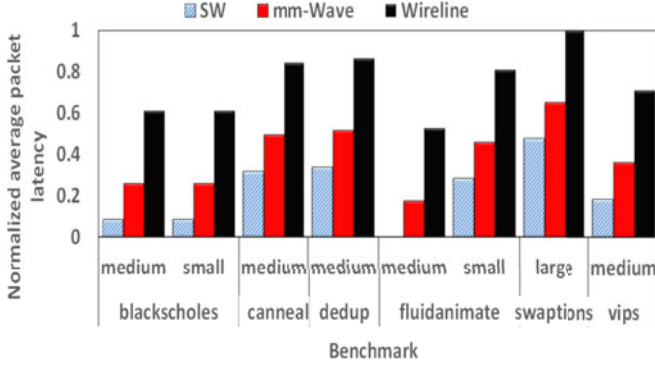
Fig. 12. Normalized average packet latency under PARSEC benchmark.

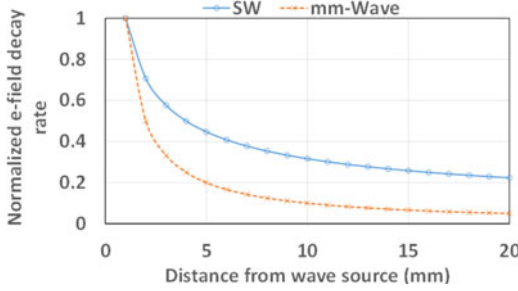Fig. 14. Average network power efficiency.

Fig. 13. Comparison of electric field decay rate of mm-Wave and SW.

dynamic power consumption by an average of 20 percent compared to mm-Wave.

Therefore, the proposed surface wave communication fabric has more promising power efficiency for long distance communications in WiNoCs compared to traditional mm-Wave.

7.4 Effect Wireless Channel on the Reliability of WiNoCs

To understand the effect of the wireless channel on the total reliability of WiNoCs, the performance evaluation of the mm-wave wireless channel is carried out by investigating the realistic channel model proposed in Section 3. We compare with conventional channel model where signals are transmitted over pure air with no MAA (e.g., two-ray channel model in [20]).[8]

The simulation is implemented in MATLAB and the parameters of various gas compositions are obtained from the HITRAN database [18]. The impacts of the transmission medium and various channel environment parameters on the performance of mm-Wave WiNoC in terms of path loss and channel capacity are evaluated with respect to different channel modeling approaches.

First, we investigate the impacts of antenna transmission frequency on the wireless channel model. Fig. 15a plots the

variation of the total path loss (i.e., L) of the two considered channel models with transmission frequency at $\mathcal{C}_{\mathcal{T}}$. Two cores $\mathcal{C}_{\mathcal{T}}$ and $\mathcal{C}_{\mathcal{R}}$ (i.e., d_C) are implemented on a chip with a die size of 20 mm^2 and the height (i.e., h) of 1 mm. The distance between $\mathcal{C}_{\mathcal{T}}$ and $\mathcal{C}_{\mathcal{R}}$ (i.e., d) is set to be 0.1 mm, satisfying $d < d_C\sqrt{2}$. Each core deploys a zigzag antennas having an elevated height of 0.02 mm (i.e., $h_T = h_R = 0.02$mm). The transmission frequency of the antennas (i.e., f) is assumed to vary in the range from 55 to 65 GHz. The system electronic noise temperature (i.e., T_S) is 296 K and the ambient pressure applied on the chip (i.e., p) is 1atm.

It can be observed in Fig. 15a that the realistic channel model for WiNoCs results in a higher total path loss compared to the conventional channel model. Also, the total path loss is shown to not monotonically increase at the GHz frequency band due to the fact that the MAA is caused by isotopologues of gases having various absorption coefficients at various frequencies. For example, the MAA causes a very high path loss at about 61.6 GHz. These observations confirm the statements in Remarks 1 and 2 regarding the effectiveness of the proposed channel model with environment-aware property.

The impacts of operating temperature of the chip on the channel of WiNoC are shown in Fig. 15b, where the total path loss of the proposed and the conventional channel models is plotted against the system electronic noise temperature (i.e., T_S) with respect to two different values of frequency band (i.e., $f = 60$ GHz and $f = 64$ GHz). It can be observed that the system temperature does not have any effects in the conventional channel model with only FSSL, while the total path loss in the proposed channel model is shown to decrease as the temperature increases at both frequency bands. This observation accordingly verifies the statement in Remark 2 on the monotonically decreasing total path loss over the system temperature due to the MAA. Taking the ambient pressure of WiNoCs into consideration, Fig. 15c plots the total path loss of various channel models versus the ambient pressure (i.e., p in kPa[9]) applied on the chip package. It can be seen in Fig. 15c that the total path loss in the conventional channel model is independent of the ambient pressure. However, the total path loss in the proposed channel model for practical WiNoC is shown to exponentially increase as the ambient pressure increases, which

---

8. In our model, the medium compositions consist of water vapour (which could also an effect of emerging liquid cooling technology), carbon dioxide, oxygen, nitrogen, ozone, molecular hydrogen, nitrous oxide, methane, dioxygen, nitrogen oxide, sulfur dioxide, acetylene, ethane, ethylene, methanol, hydrogen cyanide, chloromethane, hydroxyl radical, hydrogen chloride, chlorine monoxide, carbonyl sulfide, formaldehyde, hypochlorous acid, hydrogen peroxide, phosphine, carbonyl fluoride, sulfur hexafluoride, hydrogen sulfide, formic acid, hydroperoxyl radical, chlorine nitrate, nitrosonium ion, hypobromous acid, bromomethane, acetonitrile, carbon tetrafluoride, diacetylene, cyanoacetylene, carbon monosulfide, sulfur trioxide.
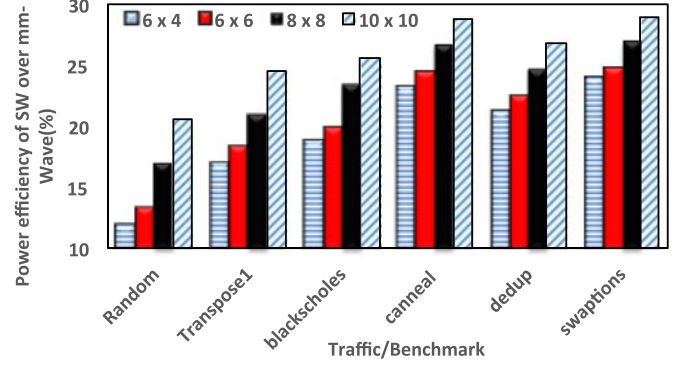
9. Note that 1atm = 101.325 kPa.

(a) Total path loss versus frequency

(b) Total path loss versus system electronic noise temperature at different frequencies

(c) Total path loss versus ambient pressure at different frequencies

(d) Channel capacity versus transmission distance at different temperatures

(e) Total path loss versus transmission distance at different frequencies

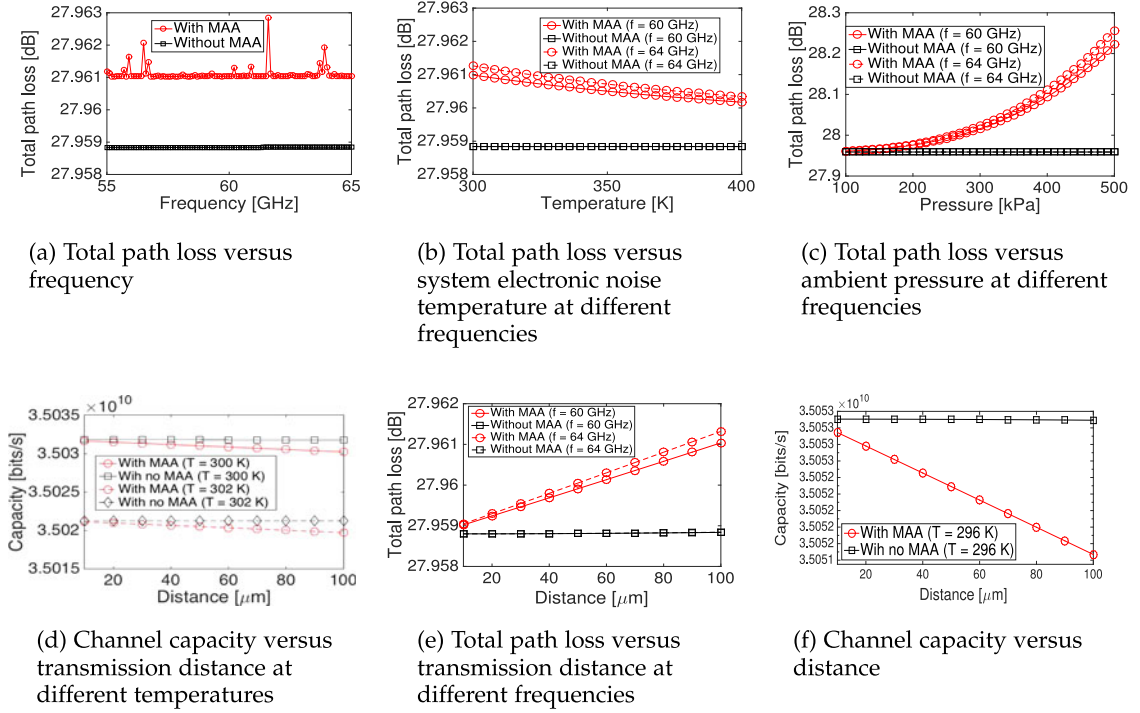(f) Channel capacity versus distance

Fig. 15. Variation of total path loss and channel capacity between mm-Wave antennas at different on-chip constraints.

confirms the claim of the exponentially increased total path loss over the ambient pressure in Remark 2. It is noted that, although there is a small difference in terms of total path loss when varying temperature, frequency and/or ambient pressure, such small changes result in a considerable difference in the achievable capacity. For instance, as shown in Fig. 15d, it can be observed that the capacity decreases more than 10 Mbits/s as the temperature slightly changes from 300 to 302 K. A similar effect can be observed when either the frequency and/or ambient pressure changes. Considering the impact of distance between two cores on the performance of WiNoC, in Fig. 15e, the total path loss of various channel models is plotted. We consider the transmission distance between $\mathcal{C}_T$ and $\mathcal{C}_R$ (i.e., d) with respect to two values of frequency $f = 60$ GHz and $f = 64$ GHz. The distance d is assumed to vary in the range $[10 : 100]\,\mu s$ and the other simulation parameters are similarly set as in Fig. 15a. It can be observed that the total path loss in both the proposed and the conventional channel models increases as the distance increases, which could be straightforwardly verified from the path loss expression in (17). However, there is only a slightly increase of the path loss in the conventional model at the GHz frequency band, while such increase is shown to be significant with a much higher path loss in the proposed channel model, which is in fact caused by the consideration of the MAA to reflect the practical WiNoC.

We investigate the impacts of MAA in the proposed channel model on the achievable channel capacity of WiNoCs. Fig. 15f plots the channel capacity against the distance between two cores $\mathcal{C}_T$ and $\mathcal{C}_R$. Similarly, two channel models including the proposed and the conventional models are considered for comparison and the parameters are set as in Fig. 15e. The antennas are assumed to operate at

frequency $f = 60$ GHz. As shown in Fig. 15f, the channel capacity in the proposed channel model for the practical WiNoCs is lower than that in the conventional channel model, even when the distance between two cores is less than 0.01 mm. This observation can be intuitively verified through the impacts of the transmission distance on the total path loss.

8 CONCLUSION AND FUTURE WORK

In this paper, a reliable 2-D waveguide communication fabric is proposed to alleviate the performance degradation due to high error rates of the wireless communication channel in hybrid wired-wireless NoCs. The TM characteristics for reliable surface wave signal propagation in the proposed communication fabric is evaluated. As a result, a thin metal layer coated with Taconic RF-43 dielectric material is designed as the 2-D wireless communication medium. A low noise quarter-wave transducer is then proposed as the interface between the SoC blocks and the wireless interface. Experiments conducted in HFSS show that, the proposed transducer has a significantly high bandwidth (45-60 GHz). Finally, the performance effect of introducing the proposed wireless communication fabric in hybrid wired-wireless NoCs is evaluated by cycle-accurate simulations. The experimental results show significant reductions in the average packet delay and power consumption compared to millimeter wave hybrid wired-wireless NoCs with both adaptive and deterministic routing techniques. Future work includes a realistic channel model for the proposed 2-D wireless communication medium, optimized WiNoC for multicast and cache coherence protocols in chip multiprocessors (CMPs), as well as a low area coding scheme to reduce network congestion due to erroneous transmission along existing lossy wireless channels for NoCs.

REFERENCES

[1] A. Ganguly, P. Pande, B. Belzer, and A. Nojeh, "A unified error control coding scheme to enhance the reliability of a hybrid wireless network-on-chip," in *Proc. IEEE Int. Symp. Defect Fault Tolerance VLSI Nanotechnology Syst.*, 2011, pp. 277–285.

[2] M. O. Agyeman, A. Ahmadinia, and A. Shahrabi, "Heterogeneous 3d network-on-chip architectures: Area and power aware design techniques," *J. Circuits Syst. Comput.*, vol. 22, no. 4, ,2013, Art. no. 1350016.

[3] M. O. Agyeman, A. Ahmadinia, and N. Bagherzadeh, *IEEE Transactions on Parallel and Distributed Systems*.

[4] S. Lee, et al., "A scalable micro wireless interconnect structure for cmps," in *Proc. 15th Annu. Int. Conf. Mobile Comput. Netw.*, 2009, pp. 217–228.

[5] X. Yu, S. Sah, S. Deb, P. Pande, B. Belzer, and D. Heo, "A wideband body-enabled millimeter-wave transceiver for wireless network-on-chip," in *Proc. Int. Midwest Symp. Circuits Syst.*, 2011, pp. 1–4.

[6] C. Xiao, Z. Huang, and D. Li, "A tutorial for key problems in the design of hybrid hierarchical NoC architectures with wireless/ RF," *Smart Comput. Rev.*, vol. 3, no. 6, pp. 425–436, 2013.

[7] K. Chang, S. Deb, A. Ganguly, X. Yu, S. P. Sah, P. P. Pande, B. Belzer, and D. Heo, "Performance evaluation and design tradeoffs for wireless network-on-chip architectures," *J. Emerg. Technol. Comput. Syst.*, vol. 8, no. 3, 23:1–23:25, 2012.

[8] Y. Xue and P. Bogdan, "User cooperation network coding approach for noc performance improvement," in *Proc. 9th Int. Symp. Networks-on-Chip*, 2015, pp. 17:1–17:8.

[9] Z. Qian, P. Bogdan, G. Wei, C.-Y. Tsui, and R. Marculescu, "A traffic-aware adaptive routing algorithm on a highly reconfigurable network-on-chip architecture," in *Proc. 8th IEEE/ACM/IFIP Int. Conf. Hardware/Software Codesign Syst. Synth.*, 2012, pp. 161–170.

[10] M. O. Agyeman, A. Ahmadinia, and A. Shahrabi, "Efficient routing techniques in heterogeneous 3d networks-on-chip," *Parallel Comput.*, vol. 39, no. 9, pp. 389–407, 2013.

[11] H. Matsutani, et al., "A case for wireless 3d nocs for cmps," in *Proc. 18th Asia and South Pacific Des. Autom. Conf*, 2013, pp. 23–28.

[12] A. Karkar, R. Al-Dujaily, A. Yakovlev, K. Tong, and T. S. T. Mak, "Surface wave communication system for on-chip and off-chip interconnects," in *Proc. 5th Int. Workshop Netw. Chip Archit*, 2012, pp. 11–16.

[13] *Taconic rf-41, rf-43, rf-45 datasheet*. [Online]. Available: http://www.taconic-add.com/pdf/rf43.pdf. Accessed on: Feb. 2015.

[14] J. Lin, et al., "Communication using antennas fabricated in silicon integrated circuits," *IEEE J. Solid-State Circuits*, vol. 42, no. 8, pp. 1678–1687, Aug. 2007.

[15] S. Deb, A. Ganguly, P. Pande, B. Belzer, and D. Heo, "Wireless NoC as interconnection backbone for multicore chips: Promises and challenges," *IEEE J. Emerging Selected Top. Circuits Syst.*, vol. 2, no. 2, pp. 228–239, Jun. 2012.

[16] V. Vijayakumaran, M. P. Yuvaraj, N. Mansoor, N. Nerurkar, A. Ganguly, and A. Kwasinski, "CDMA enabled wireless network-on-chip," *J. Emerg. Technol. Comput. Syst.*, vol. 10, no. 4, pp. 28:1–28:20, 2014.

[17] D. Matolak, S. Kaya, and A. Kodi, "Channel modeling for wireless networks-on-chips," *IEEE Commun. Mag.*, vol. 51, no. 6, pp. 180–186, Jun. 2013.

[18] "The {HITRAN2012} molecular spectroscopic database," *J. Quantitative Spectroscopy Radiative Transfer*, vol. 130, pp. 4–50, 2013.

[19] T. G. Kyle, Atmospheric Transmission, Emission and Scattering. New York, NY, USA: Pergamon, 1991.

[20] T. Rappaport, *Wireless Communications: Principles and Practice*. Jersey, NJ, USA, Prentice Hall PTR, 2001.

[21] R. M. Goody and Y. L. Yung, *Atmospheric Radiation: Theoretical Basis*. New York, NY, USA, Oxford Univ. Press, 1989.

[22] I. S. Gradshteyn and I. M. Ryzhik, *Table of Integrals, Series, and Products*. San Francisco, CA: Academic, 2007.

[23] J. Hu and R. Marculescu, "Application-specific buffer space allocation for networks-on-chip router design," in *Proc. IEEE/ACM Int. conf. Comput. Aided Des.*, 2004, pp. 354–361.

[24] R. Ling, J. Scholler, and P. Y. Ufimtsev, "The propagation and excitation of surface waves in an absorbing layer - abstract," *J. Electromagn. Waves Appl.*, vol. 12, no. 7, pp. 883–884, 1998.

[25] J. Wan, K. F. Tong, and C. Wu, "The excitation efficiency of surface waves on a reactive surface by a finite vertical aperture," in *Proc. IEEE Int. Symp. Antennas Propag. USNC/URSI Natl. Radio Sci. Meeting*, 2015, pp. 1634–1635.

[26] R. Bahri, A. Abdipour, and G. Moradi, "Analysis and design of new active quasi circulator and circulators," *Progress Electromagn. Res.*, vol. 96, pp. 377–395, 2009.

[27] M. Ravenstahl and M. Kopp, "Application brief: ANSYS HFSS for ECAD, ansys," 2013.

[28] N. Binkert, R. Dreslinski, L. Hsu, K. Lim, A. Saidi, and S. Reinhardt, "The m5 simulator: Modeling networked systems," *IEEE Micro*, vol. 26, no. 4, pp. 52–60, Jul./Aug. 2006.

[29] C. Bienia, S. Kumar, J. P. Singh, and K. Li, "The parsec benchmark suite: Characterization and architectural implications," in *Proc. 17th Int. Conf. Parallel Archit. Compilation Tech.*, 2008, pp. 72–81.

[30] J. Hestness, B. Grot, and S. W. Keckler, "Netrace: Dependency-driven trace-based network-on-chip simulation," in *Proc. 3rd Int. Workshop Netw. Chip Archit.*, 2010, pp. 31–36.

[31] M. C. F. Chang, J. Cong, A. Kaplan, C. Liu, M. Naik, J. Premkumar, G. Reinman, E. Socher, and S. W. Tam, "Power reduction of cmp communication networks via rf-interconnects," in., 2008, pp. 376–387.

Michael Opoku Agyeman received the PhD from the Department of Computing at Glasgow Caledonian University (GCU), Glasgow, in 2014. From 2014-2015, he was with the Intel Embedded System Research group of the Chinese University of Hong Kong (CUHK) as a research associate. Currently he is a lecturer at the Department of Computing and Immersive Technologies at the University of Northampton. His research interests include VLSI SoC design, wired, and wireless NoCs. He is a member of the IEEE.

Quoc-Tuan Vien received the PhD degree from GCU, Glasgow, UK., in 2012, all in radio engineering. In 2013, he worked as postdoctoral research assistant with the School of Science and Technology, Nottingham Trent University, Nottingham, U.K. He is currently a lecturer in computing & communications engineering with the School of Science and Technology, Middlesex University, London, UK. His research interests include MIMO techniques, network coding, relay networks and cognitive radio networks. He is a member of the IEEE.

Ali Ahmadinia received the PhD degree from University of Erlangen-Nuremberg, Germany, in 2006. In 2004-2005, he worked as a research associate in Electronic imaging group, Fraunhofer Institute - Integrated Circuits (IIS), Erlangen, Germany. In 2006-2008, he was a research fellow in the School of Engineering and Electronics, University of Edinburgh, Edinburgh, UK. In 2008, he joined GCU, Glasgow, UK, where he was a senior lecturer in embedded systems. He is currently a faculty member of Department of Computer Science in California State University San Marcos, US. His research has resulted more than 100 international journal and conference publications in the areas of reconfigurable computing and system-on-chip design, wireless and DSP applications. He is a member of the IEEE.

Alexandre Yakovlev received DSc from New-castle University in 2006, and MSc and PhD from St. Petersburg Electrical Engineering Institute in 1979 and 1982 respectively, where he worked in the area of asynchronous and concurrent systems since 1980, and in the period between 1982 and 1990 held positions of assistant and associate professor at the Computing Science Department. Since 1991 he has been at the Newcastle University, where he is a professor and leads the Microelectronic Systems Design research group at the School of Electrical and Electronic Engineering. He has chaired program committees of several international conferences. His dream fellow of EPSRC, United Kingdom, to investigate different aspects of energy-modulated computing. He has published four monographs and more than 300 papers, and has managed more than 25 research contracts. He is a senior member of the IEEE.

Kin-Fai Tong received the PhD degree in electronic engineering from City University of Hong Kong in 1997. He then worked in the Department as a research fellow for two years. Afterwards he worked as an expert researcher in the Photonic Information Technology Group and Millimetre-wave Devices Group of National Institute of Information and Communications Technology (NiCT), Japan. In 2005, he started his academic career in the Department of Electronic and Electrical Engineering, UCL, as a lecturer. He is a member of the IEEE.

Terrence Mak recevied the PhD from Imperial College London, in 2009. He was also a visiting research student at MIT (2004-2005). He worked as a lecturer at Newcastle University, from 2010 to 2012 . He is an associate professor in electronic and computer science, at the University of Southampton. Previously, he was with the Department of Computer Science and Engineering, as an assistant professor at CUHK, from 2012 to 2015. His current research focuses on many-core and VLSI systems design, and embedded systems engineering. His researches are supported by EPSRC, TSB and The Royal Society.. He is a member of the IEEE.